PHYSICAL REVIEW D **88,** 054502 (2013)

New representation of the Adler function for lattice QCD

Anthony Francis, Benjamin Jäger, Harvey B. Meyer, and Hartmut Wittig
PRISMA Cluster of Excellence, Institut für Kernphysik and Helmholtz Institut Mainz, Johannes Gutenberg-Universität Mainz, D-55099 Mainz, Germany
(Received 21 June 2013; published 4 September 2013)

We address several aspects of lattice QCD calculations of the hadronic vacuum polarization and the associated Adler function. We implement a representation derived previously which allows one to access these phenomenologically important functions for a continuous set of virtualities, irrespective of the flavor structure of the current. Secondly, we present a theoretical analysis of the finite-size effects on our particular representation of the Adler function, based on the operator product expansion at large momenta and on the spectral representation of the Euclidean correlator at small momenta. Finally, an analysis of the flavor structure of the electromagnetic current correlator is performed, where a recent theoretical estimate of the Wick-disconnected diagram contributions is rederived independently and confirmed.

DOI: 10.1103/PhysRevD.88.054502 PACS numbers: 12.38.Gc, 13.40.Em, 13.66.Bc, 14.60.Ef

I. INTRODUCTION

The hadronic vacuum polarization, that is, the way hadrons modify the propagation of virtual photons, is of great importance in precision tests of the Standard Model of particle physics. It enters, for instance, the running of the QED coupling constant. Together with the Higgs mass, the latter can be used to predict the weak mixing angle, which can also be measured directly, thus providing for a test. Secondly, it currently represents the dominant uncertainty in the Standard Model prediction of the anomalous magnetic moment of the muon. Given the upcoming experiment at FermiLab that is expected to improve the accuracy of the direct measurement by a factor of 4, it is important to reduce the uncertainty on the prediction by a comparable factor. While the phenomenological determination of the leading hadronic contribution is still the most accurate approach, a purely theoretical prediction is both conceptually desirable and provides for a completely independent check. Since the vacuum polarization is inserted into an integral that is strongly weighted to the low-energy domain, calculating the hadronic vacuum polarization has become an important goal for several lattice QCD collaborations performing nonperturbative simulations [1–6].

One of the features of the numerical lattice QCD framework is that the theory is formulated in Euclidean space of finite extent. Typically the theory is set up on a four-dimensional torus. The limitation of Euclidean correlation functions in finite volume to discrete values of the momenta has drawn considerable attention recently [7–9]. Many low-energy quantities defined in infinite volume, such as the slope of the Adler function at the origin or the proton radius defined from the slope of its electric form factor at $Q^2 = 0$, do not have a unique, canonical definition in finite volume. Instead, different finite-volume representations can be defined, all of which converge to the desired infinite-volume quantity. From the point of view of lattice QCD simulations, a desirable feature of such a representation is that it converges rapidly to the infinite-volume quantity. A different representation can, in general, be obtained by deriving an equivalent formulation of the infinite-volume quantity, and then carrying it over to the finite-volume theory.

Even if a new representation provides a definition of the vacuum polarization or a form factor for a continuous set of momenta, clearly it only represents progress if the finite-size effect on the final target quantity is reduced. Therefore, the merit of a new representation can only be evaluated once some theoretical understanding of the finite-size effects is reached.

Here we explore a representation of the hadronic vacuum polarization based on the time-momentum representation of the vector correlator. The starting point is Eq. (8), which was previously derived in [10]. It suggests a way to compute the hadronic vacuum polarization for any value of the virtuality. In this paper we apply the idea in a lattice QCD calculation with two light quark flavors. From the appearance of a power of the time coordinate in the integral, it is manifest that a derivative with respect to the Euclidean frequency has been taken. With a finite and periodic time extent T, the function x_0^2 is not uniquely defined. However, since it is multiplied by a vector correlation function, which falls off exponentially, the ambiguity is parametrically small. How precisely we deal with this issue is presented in Sec. V.

We address the finite-size effects on our representation of the Adler function in Sec. IV. We use the operator product expansion to analyze the finite-size effects at large Q^2, and we use the known connection between the finite-volume and the infinite-volume spectral function at low energies to study the finite-size effects at small virtualities. Even if our analysis does not apply to intermediate distances, we expect the finite-size effect coming from the long-distance part of the correlator to be the dominant one. Our results suggest that the slope of the Adler function at

the origin is approached from below in the large volume limit.

An important feature of our method is that it applies irrespective of the flavor structure of the current. The method of partially twisted boundary conditions has so far been limited to isovector quantities (see for instance [6]). Here we present a lattice calculation of the isovector contribution, which allows us to compare our results with those obtained by the commonly used momentum-space method on the same ensemble. The isovector correlator does not require the calculation of Wick-disconnected diagrams, whose standard estimators are affected by a large statistical variance. Recently, a useful estimate of the size of the latter was derived in chiral perturbation theory [11,12]. Here we revisit this relation and show that it can be understood in terms of the higher threshold at which the isosinglet channel opens compared to the isovector channel.

During the final stages of this work, a preprint by Feng *et al.* [9] appeared with which the present paper has an overlap. The authors of [9] emphasized the attractive option of accessing the hadronic vacuum polarization at small momenta with a very similar method. They also explored the interesting possibility of analytically continuing the vacuum polarization function into the timelike region below threshold.

The structure of this paper is as follows. Our definitions are collected in the next section. The finite-volume effects are analyzed in Sec. IV, with technical details to be found in the Appendix. The numerical calculation is described in Sec. V, and the results are given in Sec. VI.

II. DEFINITIONS

In this section we consider QCD in infinite Euclidean space. The vector current is defined as $j_\mu(x) = \bar{\psi}(x)\gamma_\mu\psi(x)$, where the Dirac matrices are all hermitian and satisfy $\{\gamma_\mu, \gamma_\nu\} = 2\delta_{\mu\nu}$. The flavor structure of the current will be discussed in the next section. We use capital letters for Euclidean four-momenta and lowercase letters for Minkowskian four-momenta. In Minkowski space we choose the "mostly-minus" metric convention. In Euclidean space, the natural object is the polarization tensor

$$\Pi_{\mu\nu}(Q) \equiv \int d^4x\, e^{iQ\cdot x}\langle j_\mu(x) j_\nu(0)\rangle, \tag{1}$$

and O(4) invariance and current conservation imply the tensor structure

$$\Pi_{\mu\nu}(Q) = (Q_\mu Q_\nu - \delta_{\mu\nu}Q^2)\Pi(Q^2). \tag{2}$$

With these conventions, the spectral function

$$\rho(q^2) \equiv -\frac{1}{\pi}\,\mathrm{Im}\Pi(Q^2)|_{Q_0=-iq_0+\epsilon,\boldsymbol{Q}=\boldsymbol{q}} \tag{3}$$

is non-negative for a flavor-diagonal correlator. For the electromagnetic current, it is related to the R ratio via

$$\rho(s) = \frac{R(s)}{12\pi^2}, \qquad R(s) \equiv \frac{\sigma(e^+e^- \to \text{hadrons})}{4\pi\alpha(s)^2/(3s)}. \tag{4}$$

The denominator is the tree-level cross section $\sigma(e^+e^- \to \mu^+\mu^-)$ in the limit $s \gg m_\mu^2$, and we have neglected QED corrections.

Relation (3) can be inverted. The Euclidean correlator is recovered through a dispersion relation,

$$\frac{\hat{\Pi}(Q^2)}{4\pi^2} \equiv \Pi(Q^2) - \Pi(0) = Q^2\int_0^\infty ds\,\frac{\rho(s)}{s(s+Q^2)}. \tag{5}$$

Finally we introduce the mixed-representation Euclidean correlator,

$$G(x_0)\delta_{k\ell} = -\int d^3\boldsymbol{x}\,\langle j_k(x) j_\ell(0)\rangle, \tag{6}$$

which has the spectral representation [10]

$$G(x_0) = \int_0^\infty d\omega\,\omega^2\rho(\omega^2)e^{-\omega|x_0|}, \quad x_0 \neq 0. \tag{7}$$

The vacuum polarization can be expressed as an integral over $G(x_0)$ [10],

$$\Pi(Q_0^2) - \Pi(0) = \int_0^\infty dx_0 G(x_0)\left[x_0^2 - \frac{4}{Q_0^2}\sin^2\left(\frac{1}{2}Q_0x_0\right)\right]. \tag{8}$$

From here, the Adler function is given by

$$\begin{aligned} D(Q_0^2) &\equiv 12\pi^2 Q_0^2\frac{d\Pi}{dQ_0^2} \\ &= \frac{12\pi^2}{Q_0^2}\int_0^\infty dx_0 G(x_0)(2 - 2\cos(Q_0x_0) \\ &\quad - Q_0x_0\sin(Q_0x_0)). \end{aligned} \tag{9}$$

The slope of the Adler function at the origin is of particular interest,

$$D'(0) = \lim_{Q^2\to 0}\frac{D(Q^2)}{Q^2} = \pi^2\int_0^\infty dx_0\, x_0^4\, G(x_0). \tag{10}$$

For instance, in the case of the electromagnetic current, the hadronic contribution a_ℓ^{HLO} to the anomalous magnetic moment of a lepton is given, in the limit of vanishing lepton mass, by [10]

$$\lim_{m_\ell\to 0}\frac{a_\ell^{\mathrm{HLO}}}{m_\ell^2} = \frac{1}{9}\left(\frac{\alpha}{\pi}\right)^2 D'(0). \tag{11}$$

III. ON THE FLAVOR STRUCTURE IN THE $N_f = 2$ THEORY

For simplicity we consider isospin-symmetric two-flavor QCD. The electromagnetic current is then given by $j_\mu^\gamma = j_\mu^\rho + \frac{1}{3}j_\mu^\omega$ with

$$j^{\rho}_{\mu} \equiv \frac{1}{2}(\bar{u}\gamma_\mu u - \bar{d}\gamma_\mu d), \quad j^{\omega}_{\mu} \equiv \frac{1}{2}(\bar{u}\gamma_\mu u + \bar{d}\gamma_\mu d). \quad (12)$$

For each of these currents $f = \rho$, ω, γ, we define polarization tensors $\Pi^{ff'}_{\mu\nu}$ as in Eq. (1). Obviously, only two are linearly independent, and in particular

$$\Pi^{\gamma\gamma}_{\mu\nu}(q) = \Pi^{\rho\rho}_{\mu\nu}(q) + \frac{1}{9}\Pi^{\omega\omega}_{\mu\nu}(q). \quad (13)$$

A very interesting relation was recently obtained [11] between the contributions of the Wick-connected diagrams and the Wick-disconnected diagrams in $\Pi^{\gamma\gamma}_{\mu\nu}(q)$, similar to Eq. (19) below. The derivation was based on an NLO calculation in chiral perturbation theory (ChPT), and extended to include the strange quark [12]. Here we rederive the result in a different way without relying on ChPT. In terms of Wick contractions, the Euclidean correlators are given by

$$\Pi^{\rho\rho}_{\mu\nu}(q) = \frac{1}{2}\Pi^{\mathrm{wc}}_{\mu\nu}(q), \quad (14)$$

$$\Pi^{\omega\omega}_{\mu\nu}(q) = \frac{1}{2}\Pi^{\mathrm{wc}}_{\mu\nu}(q) + \Pi^{\mathrm{wd}}_{\mu\nu}(q), \quad (15)$$

$$\Pi^{\gamma\gamma}_{\mu\nu}(q) = \frac{5}{9}\Pi^{\mathrm{wc}}_{\mu\nu}(q) + \frac{1}{9}\Pi^{\mathrm{wd}}_{\mu\nu}(q), \quad (16)$$

where "wc" and "wd" stand for Wick-connected and Wick-disconnected diagrams, respectively.

By linearity, spectral functions corresponding to $\Pi^{\mathrm{wc}}_{\mu\nu}$ and $\Pi^{\mathrm{wd}}_{\mu\nu}$ can be defined as in Eqs. (2) and (3) although $\rho^{\mathrm{wd}}(s)$ is then not necessarily positive definite. In the isovector channel, the threshold opens at $\sqrt{s} = 2m_\pi$, therefore by Eq. (14), $\rho^{\mathrm{wc}}(s)$ becomes nonzero at the same center-of-mass energy. In the isosinglet channel it opens at $\sqrt{s} = 3m_\pi$,

$$\rho^{\omega\omega}(s) = 0, \quad 0 < \sqrt{s} < 3m_\pi. \quad (17)$$

In terms of the Wick contractions, this means, from Eq. (15)

$$\rho^{\mathrm{wd}}(s) = -\frac{1}{2}\rho^{\mathrm{wc}}(s), \quad \sqrt{s} < 3m_\pi. \quad (18)$$

In particular, from Eq. (16), the contribution of the Wick-disconnected contribution to the Wick-connected contribution in the electromagnetic current spectral function is given by

$$\frac{\frac{1}{9}\rho^{\mathrm{wd}}(s)}{\frac{5}{9}\rho^{\mathrm{wc}}(s)} = -\frac{1}{10}, \quad 2m_\pi < \sqrt{s} < 3m_\pi. \quad (19)$$

This result is exact in two-flavor QCD with isospin symmetry. The derivation shows that it stems essentially from the higher energy threshold at which it becomes possible to produce an isosinglet state. Because experimental e^+e^- data shows that the three-pion channel opens rather slowly (the ω resonance is very narrow), relation (19) can be expected to be a good approximation at least up to 700 MeV. For instance the contribution to the R ratio of the $\pi^+\pi^-\pi^0$ channel to the $R(s)$ ratio is of order 0.01 at $\sqrt{s} = 700$ MeV [13], while the $R(s)$ ratio itself lies between 4.0 and 5.0 at the same center-of-mass energy. The smallness of the ratio (19) stems mainly from the small charge factor multiplying the Wick-disconnected contribution in (16).

The relation (18) between the Wick-disconnected and the Wick-connected contribution can be translated back into the Euclidean correlator via the dispersion relation (5). A stronger statement can be made in the time-momentum representation (6), since the low-energy part of the spectral function dominates exponentially at large Euclidean time separations. For $x_0 \to \infty$ we have

$$G^{\mathrm{wd}}(x_0) = -\frac{1}{2}G^{\mathrm{wc}}(x_0)(1 + \mathrm{O}(e^{-m_\pi x_0})). \quad (20)$$

Unlike at short distances, where $G^{\mathrm{wd}}/G^{\mathrm{wc}}$ is of order α_s^3 [14], the Wick-disconnected diagram is thus of the same order as the Wick-connected diagram at long distances.

The argument just presented can be made for other symmetry channels and can be extended to include the other quark flavors.

IV. FINITE-SIZE EFFECTS ON THE ADLER FUNCTION

In this section we investigate the finite-size effects on the Adler function specifically for the representation (9), although the methods used are more generally applicable.

A. Large momenta

We denote by $\Pi_{\mu\nu}(Q, L, T)$ the polarization tensor on an $T \times L^3$ torus to distinguish it from its infinite-volume counterpart $\Pi_{\mu\nu}(Q)$, and by $\Delta\Pi_{\mu\nu}(Q, L, T) \equiv \Pi_{\mu\nu}(Q, L, T) - \Pi_{\mu\nu}(Q)$ the finite-size effect (we will use the same notational convention for other quantities). Although the polarization tensor itself contains a logarithmic ultraviolet divergence, its finite-size effect is ultraviolet finite. When discussing finite-size effects, the specific finite-volume representation used must be specified [10]. Consider then the Fourier transform of $G(x_0)$. At large frequency, its finite-size effect is given by the operator product expansion,

$$\frac{1}{3}\Delta\Pi_{kk}((Q_0, \mathbf{0}), L, T) = \frac{1}{Q_0^2}\sum_{i=1}^{4} C_i(Q_0^2, \mu^2)(\langle O_4^{(i)}(\mu)\rangle_{(L,T)} - \langle O_4^{(i)}(\mu)\rangle_\infty) + \mathrm{O}(1/Q_0^4). \quad (21)$$

Dimension-four operators that contribute are the Lorentz scalar, renormalization group invariant operators $\frac{\beta(g)}{2g}G^2$

and $m\bar{\psi}\psi$, but also the (00) component of the two-flavor singlet, twist-two, dimension-four operators familiar from deep inelastic scattering. The Q^2 dependence of the Wilson coefficients $C_i(Q^2, \mu^2)$ is logarithmic. The coefficients of the Lorentz scalar operators are known to next-to-leading order [15], while the coefficients of the traceless tensor operators are known at leading order [16]. The latter can be taken from the calculation [16] performed for thermal field theory in infinite volume, since on the $T \times L^3$ torus, the expectation value of a traceless rank-two tensor operator only has one independent nonvanishing component in spite of the lack of rotational invariance in a time slice.

We thus see that the relative volume effect on the polarization tensor is suppressed by a factor Q^4. Furthermore, the finite-size effect on the expectation value of a local operator $O_4^{(i)}(\mu)$ appearing in Eq. (21) is of order $e^{-m_\pi L}$ for sufficiently large L. This fact is familiar from finite-temperature QCD. The leading finite-size effect is due to a one-particle state, so that the prefactor of $e^{-m_\pi L}$ can be related to a pion matrix element [17].

The lesson is that for momenta sufficiently large that the Fourier-transformed product of currents can be represented by a local operator, the asymptotic finite-size effects on the polarization tensor are of order $e^{-m_\pi L}$. This statement about the finite-size effect on $\Pi_{\mu\nu}$ then carries over to the Adler function at large Q^2.

B. Long-distance contribution to $D'(\mathbf{0})$

One of the most important observables is the slope $D'(0)$ of the Adler function at $Q^2 = 0$ (which up to a numerical factor coincides with the slope of the vacuum polarization). It determines the leading hadronic contribution to the anomalous magnetic moment of the electron [10], and a large fraction of the muon's anomalous magnetic moment [18]. It is theoretically attractive, because it involves no energy scale external to QCD. In the representation given in Eq. (10), the dominant contribution comes from Euclidean time separations $x_0 > 1$ fm. We, therefore, find it useful to define

$$D'_t \equiv \pi^2 \int_t^\infty dx_0\, x_0^4\, G(x_0), \tag{22}$$

so that $D'_0 = D'(0)$. In the infinite-volume theory, the contribution of the $|\pi^+\pi^-\rangle_{\text{out}}$ states with an energy up to and including the ρ mass completely dominates this contribution. Given the argument made above on the finite-size effects on the short-distance contribution to the Adler function, and the form of the finite-size effects in free field theory (see Sec. A 3), we expect the finite-size effects on $D'(0)$ to be dominated by the finite-size effects on D'_t for $t = 1$ fm. We are therefore led to discuss the latter. We first consider the case where the pion mass is set to its physical value. By assuming a specific model for the timelike pion form factor $F_\pi(\omega)$, we extend our analysis to the pion mass at which we later present numerical lattice QCD results.

If a temporal extent $T = 2L$ is chosen, as is common practice, the dominant finite-size effect comes from the finite spatial box extent. In the following theoretical analysis, we therefore set T to infinity. How to proceed in practice where T is finite is discussed in Sec. VI.

One source of finite-size effects are the polarization effects on single-particle states. They have been analyzed in detail in the past [19]. The upshot is that the properties of these states are only affected by corrections that are exponential in the linear torus size. In the following, we will neglect these finite-size corrections. In lattice QCD calculations, this assumption will have to be checked explicitly.

In [10], an analysis of the finite-size effects on $G(x_0)$ was carried out using the relation between the finite-volume spectral function and the infinite-volume spectral function [20,21]. This relation is only firmly established up to the inelastic threshold of $\omega = 4m_\pi$. Here we will be less rigorous and assume that even somewhat above this threshold, the relation remains a good approximation. The main justification for this assumption is that the ρ decays almost exclusively into two pions. We also neglect possible contributions from $\pi\pi$ scattering in the $\ell = 3$ and higher partial waves.

Before using the full machinery of Lüscher's finite-volume formalism, it is worth understanding the qualitative behavior of $\Delta D'_t$ in two simple, opposite limits. In one limit, we have noninteracting pions, $F_\pi(\omega) = 1$ and $G(x_0)$ can be computed exactly both in finite and in infinite volume. The ratio of the finite-volume to the infinite-volume correlation function is diplayed in Fig. 1. Clearly the finite-size effects are large for a typical value of $m_\pi L = 4$.

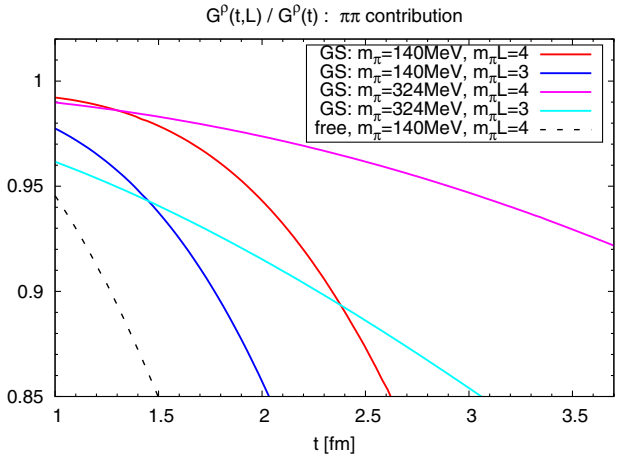

FIG. 1 (color online). Relative finite-size effect on the Euclidean correlator (6) for a pion form factor given by the Gounaris-Sakurai (GS) parametrization [once with parameters $(m_\pi = 140\,\text{MeV}, m_\rho = 773\,\text{MeV}, \Gamma_\rho = 130\,\text{MeV})$ and once with parameters $(m_\pi = 324\,\text{MeV}, m_\rho = 894\,\text{MeV}, \Gamma_\rho = 61\,\text{MeV})$], and for free pions. For details see Appendix A.

TABLE I. The first eight energy levels and matrix elements on a torus of linear size $L = 4/m_\pi$ for the Gounaris-Sakurai parametrization of $F_\pi(\omega)$ at the physical pion mass (see Appendix A; $\omega \equiv 2\sqrt{m_\pi^2 + k^2}$). The "Lellouch-Lüscher"' factor $\mathbb{L}(k)$ and the pion form factor at the corresponding energies are given in columns 3 and 4. The last column gives, for the nth state, the sum of the contributions of the n first states to $G(t, L)$ for $t = 1$ fm and $m_\pi L = 4$, normalized by the infinite-volume correlator $G(t)$.

k/m_π	$\lvert A\rvert^2/m_\pi^3$	$\mathbb{L}(k)$	$\lvert F_\pi(\omega)\rvert^2$	$\frac{G_{\le n}(t,L)}{G(t)}$
1.548	0.0737	6.606	3.507	0.092
2.133	0.4702	11.53	12.85	0.378
2.559	1.1333	28.95	42.52	0.772
2.831	0.7509	23.09	16.21	0.954
3.171	0.1124	62.41	4.558	0.971
3.581	0.1452	25.13	1.615	0.984
3.912	0.1335	19.36	0.867	0.9916
4.459	0.0192	91.10	0.391	0.9921

In the other limit, the pion interactions are such that the vector current only couples to a stable ρ meson, $\rho(s) = F_\rho^2 \delta(s - m_\rho^2)$. This limit correspond to the expected behavior at very large number of colors N_c. In this case, $G(x_0, L) = \frac{1}{2} F_\rho^2 m_\rho e^{-m_\rho x_0}$. The only finite-volume effect in this case stems from the finite-size effects on m_ρ and F_ρ, which are exponentially small in the volume. Thus in this limit the finite-size effects are expected to be much more benign.

Experimental e^+e^- data shows that QCD lies somewhere in between these two extremes, but is somewhat closer to the narrow resonance limit. Using the Gounaris-Sakurai parametrization of the timelike pion form factor [22] at the physical pion mass, we have calculated the eight lowest energy eigenstates for $m_\pi L = 3$ and 4 and their coupling to the isospin current using the results of [20,21] (see Table I). For details of the calculation, we refer the reader to Appendix A. Together these states saturate the correlator beyond 1 fm to a high degree of accuracy (see the last column of Table I). The ratio $G(x_0, L)/G(x_0)$ is displayed in Fig. 1. Although the relative finite-size effect grows rapidly at long distances, for $m_\pi L = 4$ it is of acceptable size at the distances which dominate $D'(0)$ (compare with Fig. 4). Finally, Table II gives the finite-size effect on D_t' for $t = 1$ fm. With $m_\pi L = 4$, the effect amounts to 7%, which is a larger effect than is observed for many mesonic observables.

We also note that at the heavier quark masses currently studied in the simulations, the ρ is narrower and the finite-size effect for the same value of $m_\pi L$ is therefore smaller in the Euclidean time range where the ρ dominates. This point is illustrated in Fig. 1 for $m_\pi = 324$ MeV, where we used the Gounaris-Sakurai parametrization with the parameters $m_\rho = 894$ MeV and $\Gamma_\rho = 61$ MeV. The latter value is obtained by assuming that $\Gamma_\rho \propto k_\rho^3/m_\rho^2$ [20], where k_ρ is the momentum of a pion in the decay $\rho \to \pi\pi$.

TABLE II. The relative finite-size effect $D_t'(L)/D_t'$ for $t = 1$ fm and $m_\pi = 140$ MeV [see Eqs. (22) and (9)].

$m_\pi L$	GS	Free pions
3	0.853	0.429
4	0.927	0.671
5	0.961	0.828

V. NUMERICAL SETUP

In this and the following sections, we describe a numerical implementation of the representation of the vacuum polarization and Adler function given in Eqs. (8) and (9). In particular, we show how the integral over the time coordinate can be treated without introducing unnecessarily large finite time-extent effects. We restrict ourselves to one value of the light quark mass and one lattice spacing for which we can directly compare the results obtained with the new method to those obtained with the momentum-space method [23].

All our numerical results were computed on dynamical gauge configurations with two mass-degenerate quark flavors. The gauge action is the standard Wilson plaquette action [24], while the fermions were implemented via the $O(a)$ improved Wilson discretization with nonperturbatively determined clover coefficient $c_{\rm sw}$ [25]. The configurations were generated using the DD-HMC algorithm [26,27] as implemented in Lüscher's DD-HMC package [28] and were made available to us through the coordinated lattice simulations (CLS) effort [29]. We calculated correlation functions using the same discretization and masses as in the sea sector on a lattice of size 96×48^3 (labeled F6 in [30]) with a lattice spacing of $a = 0.0631(21)$ fm [31] and a pion mass of $m_\pi = 324$ MeV, so that $m_\pi L = 5.0$.

Regarding the flavor structure, we restrict ourselves to the isovector current j_μ^ρ, normalized as in Eq. (12). On the lattice we implement the correlation function (6) as a mixed correlator between the local and the conserved current,

$$G^{\rm bare}(x_0, g_0)\delta_{kl} = -a^3 \sum_{\boldsymbol{x}} \langle J_k^c(x) J_\ell^l(0)\rangle, \tag{23}$$

where

$$J_\mu^l(x) = \bar{q}(x)\gamma_\mu q(x), \tag{24}$$

$$J_\mu^c(x) = \frac{1}{2}(\bar{q}(x + a\hat{\mu})(1 + \gamma_\mu)U_\mu^\dagger(x)q(x) - \bar{q}(x)(1 - \gamma_\mu)U_\mu(x)q(x + a\hat{\mu})). \tag{25}$$

We have renormalized the vector correlator using

$$G(x_0) = Z_V(g_0)G^{\rm bare}(x_0, g_0) \tag{26}$$

with the nonperturbative value of $Z_V = 0.750(5)$ [32]. We have not included $O(a)$ contributions from the improvement term proportional to the derivative of the antisymmetric

tensor operator [33,34]. A quark-mass dependent improvement term of the form $(1 + b_V(g_0)am_q)$ [34] was also neglected. These contributions should eventually be included to ensure a smooth scaling behavior as the continuum limit is taken. Here, our primary goal is to test the method on a single ensemble.

VI. NUMERICAL RESULTS

We begin by analyzing results for the correlator $G(x_0)$, and then show how the latter can be used to compute the subtracted vacuum polarization and the Adler function.

A. Correlator data

In Fig. 2 we show the local-conserved vector correlation function. One virtue of this discretization is that in infinite volume it leads to the property

$$\int_{-\infty}^{\infty} dx_0 G(x_0) = 0. \tag{27}$$

The correlator must drop to negative values for very small time separations in order to fulfill the above identity. Indeed we observe this negative contact term for very small time separations $|x_0| \leq a$, and Eq. (27) is satisfied by our data.

The goal is to compute $\hat{\Pi}(Q^2)$ and its derivative from the lattice correlation function using the continuum relation Eq. (8). To achieve this one has to carry out the integral over all time separations. On the lattice this is not straightforward, since only a finite number of points are available. In addition, the signal deteriorates rapidly at large time separations. It is known however that the correlation function decays exponentially for large times. Therefore, it is natural to extrapolate the local-conserved correlator with an exponential that decays with the lowest lying "mass" [35]. This mass can be fixed by fitting the lattice data to an ansatz of the form

$$G_{\text{Ansatz}}(x_0) = \sum_{n=1}^{2} |A_n|^2 e^{-m_n x_0}, \tag{28}$$

for x_0 sufficiently below $T/2$ that the "backward" propagating states make a negligible contribution. To ensure a reliable determination of this mass, we have extracted it from a separate correlation function, computed on the same configurations using smeared operators at the source and sink [31]. This correlator has greater overlap with the ground state and yields very precise data. The mass parameter determined in this way is then carried over to the local-conserved correlator and the corresponding exponential is smoothly connected to the lattice data by fitting $|A_1|^2$ to the data around $x_0 = T/4$.

The resulting correlation function is shown as the red-shaded band in Fig. 2, where the error estimates were obtained via a jackknife procedure. In the transition region from the data dominated to the extrapolation-dominated result, the errors increase for a small number of time steps on the whole; however, reasonably small errors are achieved in this way.

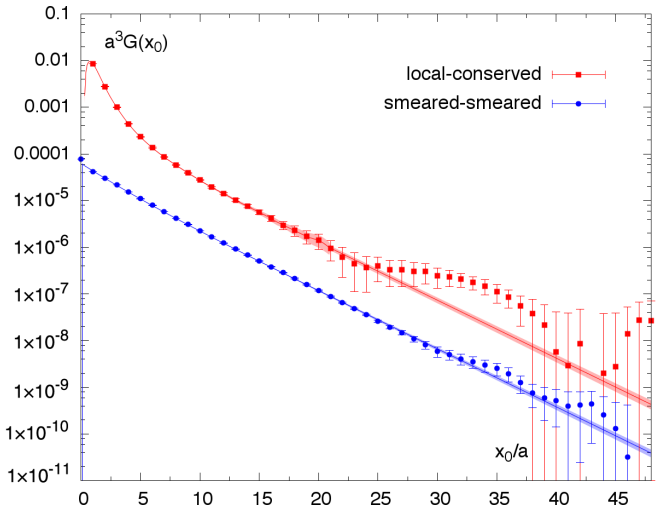

FIG. 2 (color online). Local-conserved and smeared-smeared isovector vector correlation functions. The red-shaded area shows the correlator entering Eq. (8) for the computation of $\hat{\Pi}(Q^2)$; the blue shaded area correlator is used to fit the lowest lying mass for extrapolation to all time beyond $x_0 \simeq T/4$.

B. Computing $\hat{\Pi}(Q^2)$ and its slope

In order to obtain $\hat{\Pi}(Q^2)$ given the local-conserved correlation function of Fig. 2, one has to compute its convolution with the kernel

$$K(x_0, Q_0) = x_0^2 - \frac{4\sin^2(Q_0 x_0/2)}{Q_0^2}. \tag{29}$$

Using Eq. (8), derivatives are directly accessible [see for instance Eq. (10)].

In Fig. 3 we show the result for $\hat{\Pi}(Q^2)$ and the slope $d\hat{\Pi}(Q^2)/dQ^2$, as computed from the red-shaded correlator in Fig. 2. Here all errors were computed using a jackknife method on a total of 392 measurements. Turning first to $\hat{\Pi}(Q^2)$, for comparison we show the result obtained on the same lattice using the standard method [23] with the same local-conserved discretization and comparable statistics. The latter method consists in employing Eqs. (1) and (2) to obtain first $\Pi(Q^2)$ and then determining $\Pi(0)$ via extrapolation. In this approach, the number of data points at small Q^2 was significantly increased using twisted-boundary conditions [36–38]. Still, the extrapolation $\Pi(Q^2 \to 0)$ is difficult to constrain as the signal deteriorates in this limit. The results obtained via Eq. (8) do not suffer directly from these issues, as the physically relevant quantity, $\hat{\Pi}(Q^2)$, is computed directly.

Clearly the results obtained using our new method are very well compatible with the standard method. It should be noted that the larger errors for large Q^2 only play a small role when computing a_μ^{HLO}, as the large Q^2

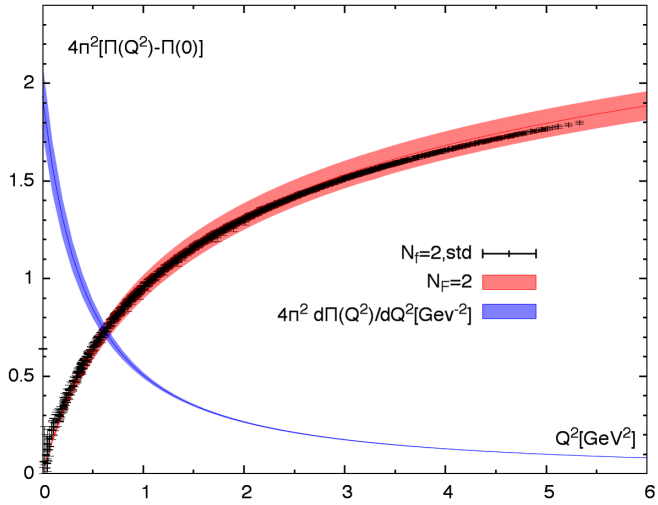

FIG. 3 (color online). The subtracted vacuum polarization $\hat{\Pi}(Q^2)$ and $d\hat{\Pi}(Q^2)/dQ^2$ computed from the red-shaded correlator in Fig. 2. The data shown in black were obtained using the momentum-space method on the same ensemble with comparable statistics [23].

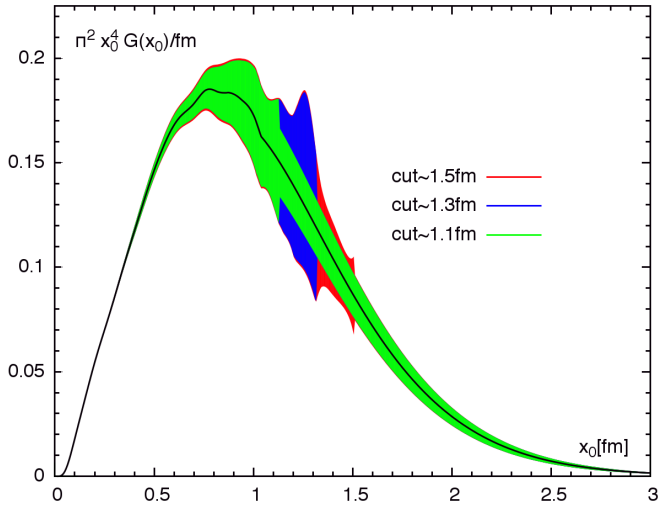

FIG. 4 (color online). The integrand needed to compute the slope $D'(0)$ of the Adler function at $Q^2 = 0$. The bands of different color are the results obtained by replacing the data by a pure exponential falloff around the value $x_0 = \text{cut}$ [fm]. The area under this curve (divided by $3 \times (0.197)^2$) is equal to the intercept of the blue curve in Fig. 3.

region is highly suppressed in the relevant integral. Using Eq. (9) we also display the slope $d\hat{\Pi}(Q^2)/dQ^2$ as a blue shaded band in Fig. 3. Throughout the result exhibits small statistical errors and the intercept at $Q^2 = 0$ can be determined relatively precisely. We find $D'(0) = 3\hat{\Pi}'(0) = 5.8(5)\ \text{GeV}^{-2}$.

The factor x_0^4 in the integral representation Eq. (10) of the derivative of the Adler function at the origin suppresses the small time region of the correlator. The impact of each x_0 region can be visualized by displaying the integrand, see Fig. 4. Here we also show the results using three different values of the transition point between the data and the extrapolation. This gives us a handle to study the effect of the onset of the fitted pure exponential described above. The effect is seen to lie within the error band, while the impact on the resulting $\hat{\Pi}(Q^2)$ and $d\hat{\Pi}(Q^2)/dQ^2$ was checked and found to be negligible. Examining the central value curve we observe that the dominant contribution to the integrand is in fact given by the region $0.5\ \text{fm} \leq x_0 \leq 1.5\ \text{fm}$. Consequently, to precisely pin down $D'(0)$ and the closely related a_μ^{HLO}, very accurate lattice data in this region are desirable.

In Fig. 5, where we show the Adler function and the vacuum polarization as a function of the virtuality, we follow the approach [4,10] of rescaling the horizontal axis using the vector meson mass. In this way one hopes to achieve an approximate scaling at small Q^2, in the sense that the curves corresponding to different quark masses approximately lie on top of each other. We compare our result to a phenomenological model (Eq. (93) of [10]) for the isovector channel, which predicts in particular $D'(0) = 9.81(30)\ \text{GeV}^{-2}$. It is an approximate parametrization of the data compiled by the Particle Data Group [39]. We estimate its overall uncertainty to be on the order of 3%–4%. The comparison is shown in Fig. 5 for the low Q^2 region of $\hat{\Pi}(Q^2)$ and the Adler function $D(Q^2)$. Even after the rescaling, the lattice data lie visibly below the phenomenological curve. A plausible origin for the remaining difference is the spectral density below the ρ mass, since the integrand to obtain $D'(0)$ is $R_1(s)/s^2$, where R_1 is the R ratio restricted to isovector final hadronic states.

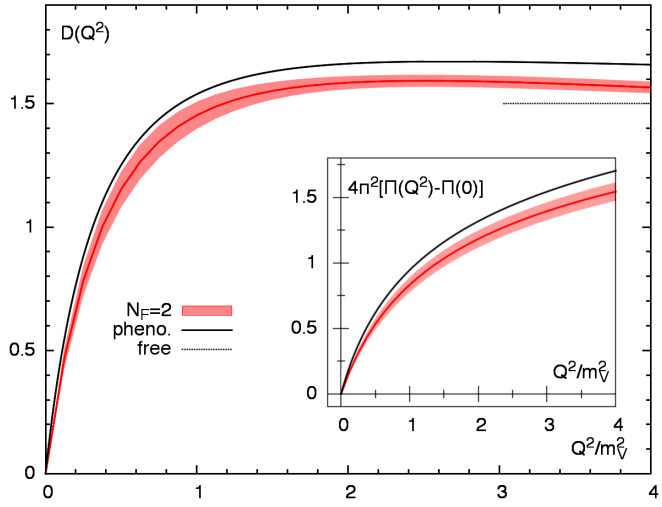

FIG. 5 (color online). The functions $\hat{\Pi}(Q^2)$ and $D(Q^2)$ from our analysis and a phenomenological model [10]. The horizontal axis has been rescaled by the ground-state mass $m_1 = 894(2)$ MeV on the lattice and the physical ρ meson mass (770 MeV), respectively. For reference the free result $D(Q^2) = \frac{3}{2}$ is shown as a dotted line.

VII. CONCLUSION

We have tested a new representation of the vacuum polarization and the Adler function $D(Q^2)$, which can be used in lattice QCD (see also [9]). For the isovector contribution, we have verified that it agrees well with the widely used method in four-momentum space. In the latter case, we have data [23] generated with twisted boundary conditions, giving access to a discrete but dense set of virtualities. By employing a representation that allows for continuous values of the momenta, it is no more difficult to extract the Adler function than the subtracted vacuum polarization. The former has the advantage of being local in Q^2, which facilitates the comparison with perturbation theory at large Q^2.

A theoretical analysis of the finite-size effects associated with $D'(0)$ suggests that the latter can be brought down to about 5% at the physical pion mass for spatial volumes $m_\pi L$ between 4 and 5. The infinite-volume quantity is approached from below. At fixed $m_\pi L$ the finite-size effect depends strongly on the width of the ρ meson, implying that it rapidly becomes a more critical issue when the pion mass is lowered towards its physical value. If the masses and couplings of the low-lying vector states can be determined on the lattice, the bulk of the finite-size effect can be corrected for [10].

In the near future we plan to combine the extensive set of data that we have generated with the standard method with the method presented here to extract the Adler function at the origin and a_μ^{HLO}. Subsequently, the calculation of the Wick-disconnected diagrams can be taken up with our new representation.

ACKNOWLEDGMENTS

We are grateful to Michele Della Morte and Andreas Jüttner, whose original code formed the basis for our analysis programs, and to our colleagues within CLS for sharing the lattice ensemble used. We thank Georg von Hippel for discussions and for providing the smeared vector correlator [31]. The correlation functions were computed on the dedicated QCD platform "Wilson" at the Institute for Nuclear Physics, University of Mainz. This work was supported by the Center for Computational Sciences as part of the Rhineland-Palatinate Research Initiative.

APPENDIX A: FINITE-SIZE EFFECTS ON THE EUCLIDEAN CORRELATOR

In this appendix we present the details of the calculation that underlies Tables I and II and Fig. 1. It is based on the two-pion contribution to the spectral function.

The $\pi\pi$ contribution to the spectral function is given by (see for instance [40])

$$\rho(\omega^2) = \frac{1}{48\pi^2}\left(1 - \frac{4m_\pi^2}{\omega^2}\right)^{\frac{3}{2}} |F_\pi(\omega)|^2. \tag{A1}$$

Charge conservation implies that $F_\pi(0) = 1$. Above the threshold $\omega = 2m_\pi$, the phase of the pion form factor is equal to the p-wave pion phase shift, $F_\pi(\omega) = |F_\pi(\omega)| e^{i\delta_{11}(k)}$ (Watson theorem).

1. Interacting pions

In infinite volume, the Euclidean correlation function is obtained using Eqs. (7) and (A1). For the finite-volume correlator, we proceed as follows.

The discrete energy levels in the box and the infinite-volume phase shifts are related by [20,41]

$$\delta_{11}(k) + \phi\left(\frac{kL}{2\pi}\right) = n\pi, \quad n = 1, 2, \ldots, \tag{A2}$$

$$\omega \equiv 2\sqrt{m_\pi^2 + k^2}. \tag{A3}$$

The function $\phi(z)$, tabulated in [20], is defined by $\tan\phi(z) = -\frac{\pi^{3/2} z}{\mathcal{Z}_{00}(1;z^2)}$, where $\mathcal{Z}_{00}(1;z^2)$ is the analytic continuation in s of $\mathcal{Z}_{00}(s;z^2) = \frac{1}{\sqrt{4\pi}} \sum_{\boldsymbol{n}\in\mathbb{Z}^3} \frac{1}{(\boldsymbol{n}^2 - z^2)^s}$. The corresponding finite-volume matrix elements for unit-normalized finite-volume states are given by [21]

$$|F_\pi(\omega)|^2 = \mathbb{L}(k) \frac{3\pi\omega^2}{2k^5} |A|^2, \tag{A4}$$

$$\mathbb{L}(k) \equiv [z\phi'(z)]_{z=\frac{kL}{2\pi}} + k\frac{\partial\delta_1(k)}{\partial k}. \tag{A5}$$

The correlation function is then obtained as

$$G(x_0, L) = \sum_n |A_n|^2 e^{-\omega_n x_0}. \tag{A6}$$

We thus only need a realistic model for the timelike pion form factor, $F_\pi(\omega)$.

2. The Gounaris-Sakurai model of F_π

The GS parametrization [22] contains two free parameters characterizing the ρ resonance—m_ρ and Γ_ρ. Defining k_ρ via $m_\rho = 2\sqrt{k_\rho^2 + m_\pi^2}$, the phase shift is written

$$\frac{k^3}{\omega} \cot\delta_{11}(k) = k^2 h(\omega) - k_\rho^2 h(m_\rho) + b(k^2 - k_\rho^2), \tag{A7}$$

$$b = -\frac{2}{m_\rho}\left[\frac{2k_\rho^3}{m_\rho\Gamma_\rho} + \frac{1}{2} m_\rho h(m_\rho) + k_\rho^2 h'(m_\rho)\right], \tag{A8}$$

$$h(\omega) = \frac{2}{\pi}\frac{k}{\omega}\log\frac{\omega + 2k}{2m_\pi}. \tag{A9}$$

The form factor is then given by

$$F_\pi(\omega) = \frac{f_0}{\frac{k^3}{\omega}(\cot[\delta_{11}(k)] - i)}, \tag{A10}$$

$$f_0 = -\frac{m_\pi^2}{\pi} - k_\rho^2 h(m_\rho) - b\frac{m_\rho^2}{4}. \tag{A11}$$

By analytic continuation, $F_\pi(\omega)$ is guaranteed to be unity at the origin. In all numerical applications, we have set $m_\pi = 139.57$, $m_\rho = 773$, and $\Gamma_\rho = 130$ MeV. These values were chosen so as to approximately match the 2010 KLOE data [42]. We have not tried to correct for isospin-breaking effects in the experimental data.

3. Noninteracting pions

We consider here the case of noninteracting pions of mass m_π. The isovector current takes the form

$$j_\mu^a(x) = \epsilon^{abc}\pi^b(x)\partial_\mu\pi^c(x) \tag{A12}$$

for pion fields with a canonically normalized kinetic term. Then one finds in finite volume, with $E_k^2 = \boldsymbol{k}^2 + m_\pi^2$,

$$G(x_0, L) = \frac{1}{L^3}\sum_{\boldsymbol{k}} k_z^2 \frac{e^{-2E_k|x_0|}}{E_k^2}. \tag{A13}$$

To evaluate the finite-volume correlator at large times, Eq. (A13) is an adequate representation. At small times, however, it is more efficient to use a different representation obtained using the Poisson formula,

$$G(x_0, L) = \frac{m_\pi^3}{6\pi^2}\sum_{\boldsymbol{n}}\int_0^\infty dx \frac{x^4}{x^2+1} \times \frac{\sin(m_\pi L|\boldsymbol{n}|x)}{m_\pi L|\boldsymbol{n}|x} e^{-2m_\pi|x_0|\sqrt{x^2+1}}. \tag{A14}$$

The $\boldsymbol{n} = 0$ term coincides with the infinite-volume result, which as a consistency check can also be obtained using Eqs. (7) and (A1) by setting $F_\pi(\omega) = 1$. In a saddle point approximation, we have

$$G(x_0, L) - G(x_0) \simeq \sqrt{\frac{m_\pi}{\pi^3|x_0|^5}}\frac{e^{-2m_\pi|x_0|}}{48}\sum_{\boldsymbol{n}\neq 0}\left(3 - \frac{m_\pi L^2\boldsymbol{n}^2}{2|x_0|}\right) \times \exp\left(-\frac{m_\pi L^2\boldsymbol{n}^2}{4|x_0|}\right). \tag{A15}$$

In this form it is clear that for fixed L, the expansion converges rapidly as long as $|x_0|$ is substantially smaller than $m_\pi L^2$. Conversely, the finite size effect is exponential for any fixed x_0, but only once L is a multiple of $\sqrt{|x_0|/m_\pi}$. Numerically, if we require that the absolute value of the exponent in the last exponential be at least 4, we get $x_0^{\max}\ [\text{fm}] \simeq \frac{197}{m_\pi[\text{MeV}]}(\frac{m_\pi L}{4})^2$. We also note that the finite-size effect is negative for large L.

[1] T. Blum, Phys. Rev. Lett. **91**, 052001 (2003).
[2] M. Göckeler, R. Horsley, W. Kürzinger, D. Pleiter, P. E. L. Rakow, and G. Schierholz (QCDSF Collaboration), Nucl. Phys. **B688**, 135 (2004).
[3] C. Aubin and T. Blum, Phys. Rev. D **75**, 114502 (2007).
[4] X. Feng, K. Jansen, M. Petschlies, and D. B. Renner, Phys. Rev. Lett. **107**, 081802 (2011).
[5] P. Boyle, L. Del Debbio, E. Kerrane, and J. Zanotti, Phys. Rev. D **85**, 074504 (2012).
[6] M. Della Morte, B. Jäger, A. Jüttner, and H. Wittig, J. High Energy Phys. 03 (2012) 055.
[7] G. de Divitiis, R. Petronzio, and N. Tantalo, Phys. Lett. B **718**, 589 (2012).
[8] C. Aubin, T. Blum, M. Golterman, and S. Peris, Phys. Rev. D **86**, 054509 (2012).
[9] X. Feng *et al.*, arXiv:1305.5878.
[10] D. Bernecker and H. B. Meyer, Eur. Phys. J. A **47**, 148 (2011).
[11] A. Jüttner and M. Della Morte, Proc. Sci. LAT2009 (2009) 143.
[12] M. Della Morte and A. Jüttner, J. High Energy Phys. 11 (2010) 154.
[13] S. Dolinsky, V. Druzhinin, M. Dubrovin, V. Golubev, V. Ivanchenko *et al.*, Phys. Rep. **202**, 99 (1991).
[14] P. Baikov, K. Chetyrkin, J. Kuhn, and J. Rittinger, J. High Energy Phys. 07 (2012) 017.
[15] K. Chetyrkin, V. Spiridonov, and S. Gorishnii, Phys. Lett. **160B**, 149 (1985).
[16] S. Mallik, Phys. Lett. B **416**, 373 (1998).
[17] H. B. Meyer, J. High Energy Phys. 07 (2009) 059.
[18] B. Brandt, M. Della Morte, B. Jäger, A. Jüttner, and H. Wittig, Prog. Part. Nucl. Phys. **67**, 223 (2012).
[19] M. Lüscher, Commun. Math. Phys. **104**, 177 (1986).
[20] M. Lüscher, Nucl. Phys. **B364**, 237 (1991).
[21] H. B. Meyer, Phys. Rev. Lett. **107**, 072002 (2011).
[22] G. Gounaris and J. Sakurai, Phys. Rev. Lett. **21**, 244 (1968).
[23] M. Della Morte, B. Jäger, A. Jüttner, and H. Wittig, Proc. Sci., LATTICE (2012) 175.
[24] K. G. Wilson, Phys. Rev. D **10**, 2445 (1974).
[25] K. Jansen and R. Sommer (ALPHA Collaboration), Nucl. Phys. **B530**, 185 (1998).
[26] M. Lüscher, Comput. Phys. Commun. **165**, 199 (2005).
[27] M. Lüscher, J. High Energy Phys. 12 (2007) 011
[28] http://luscher.web.cern.ch/luscher/DD-HMC/index.html, 2010.
[29] https://twiki.cern.ch/twiki/bin/view/CLS/WebIntro, 2010.
[30] S. Capitani, M. Della Morte, G. von Hippel, B. Jäger, A. Jüttner, B. Knippschild, H. B. Meyer, and H. Wittig, Phys. Rev. D **86**, 074502 (2012).
[31] S. Capitani, M. Della Morte, G. von Hippel, B. Knippschild, and H. Wittig, Proc. Sci., LATTICE (2011) 145.

[32] M. Della Morte, R. Hoffmann, F. Knechtli, R. Sommer, and U. Wolff, J. High Energy Phys. 07 (2005) 007.
[33] M. Lüscher, S. Sint, R. Sommer, and P. Weisz, Nucl. Phys. **B478**, 365 (1996).
[34] S. Sint and P. Weisz, Nucl. Phys. **B502**, 251 (1997).
[35] The energy level extracted in this way does not necessarily correspond to a stable vector particle.
[36] G. de Divitiis, R. Petronzio, and N. Tantalo, Phys. Lett. B **595**, 408 (2004).
[37] C. Sachrajda and G. Villadoro, Phys. Lett. B **609**, 73 (2005).
[38] P. F. Bedaque and J.-W. Chen, Phys. Lett. B **616**, 208 (2005).
[39] C. Amsler *et al.* (Particle Data Group), Phys. Lett. B **667**, 1 (2008).
[40] F. Jegerlehner and A. Nyffeler, Phys. Rep. **477**, 1 (2009).
[41] M. Lüscher, Nucl. Phys. **B354**, 531 (1991).
[42] F. Ambrosino *et al.* (KLOE Collaboration), Phys. Lett. B **700**, 102 (2011).